Variable-Structure PID Controller with Anti-Windup for Autonomous Underwater Vehicle

Minsung Kim[1], Hangil Joe[2], Juhyun Pyo[1], Jongkyoo Kim[3], Hyosin Kim[3], and Son-cheol Yu[1]
[1]the Department of Creative IT Engineering, POSTECH, Pohang, Korea
[2]Ocean Science and Technology Institute, POSTECH, Pohang, Korea
[3]the Department of Electrical Engineering, POSTECH, Pohang, Korea

***Abstract*—In practice, a PID controller has been used most commonly to control underwater vehicles. However, PID controllers suffer significant loss of performance due to integral windup when used in the system with actuator saturation. In this paper, we propose a dual-loop VSPID controller with anti-windup to reduce the integral-windup effect. We tested the proposed method using an real autonomous underwater vehicle and confirmed that the method successfully decreased the integral-windup effect.**

***Index Terms*—Dual-loop; Cyclops; controller structure.**

I. Introduction

Autonomous underwater vehicle (AUV) are increasingly important in exploring underwater environments. Typical tasks are geological surveying and data collection. For underwater surveys using AUV, precise control/attitude control is very important because the quality of obtained data is closely related to it. However, control of an AUV is difficult due to coupled nonlinearities, parameter uncertainties resulting from poor knowledge of hydrodynamic coefficients, and external disturbances such as ocean currents and waves. So, during the past few decades, a number of research results that deal with these issues have been reported.

Various control strategies have been proposed. Key approaches include PID controller [1][2], sliding mode controller [3][4], H_∞ controller [5][6], and backstepping [7].

In practical applications, the PID controller has been used most commonly among the aforementioned controllers because of its simplicity in tuning for improving performance and robustness. The decoupled PID controller was applied to AUV, developed at the Norwegian Defence Research Establishment, for steering, diving, and speed control [1]. The dual-loop PID controller has also been applied to the remotely operated vehicle (ROV), developed at the CNR-IAN Robotics Department, for speed control [2]. But these PID controllers suffer significant loss of performance due to integral windup when used in a system in which actuator saturation occurs. The integral windup may cause significant overshoot that requires a long time for recovery.

To overcome this problem, a single-loop PID controller with anti-windup has been introduced for a torpedo-type AUV [8] and a hovering-type AUV [9]. But, the anti-windup technique has not been used in the dual-loop PID controller. The dual-loop controller shows a better performance than the single-loop controller, because inner-loop controller can reduce the variation of hydrodynamics and reject disturbances quickly [10].

In this paper, we propose a dual-loop PID controller with anti-windup for AUV. The proposed control scheme consists of three elements. First, the feedback term compensates for the nonlinear part of the system. Then, the PID controller with anti-windup in the inner-loop stabilizes the dynamics in advance. Finally, the PID controller with anti-windup in the outer-loop makes the whole closed-loop system stable. The proposed controller is developed based on the variable-structure PID (VSPID) structure with anti-windup [11]. A conventional anti-windup technique prevents the integral windup by using the actuator limits only. But the anti-windup techniques in the proposed control scheme prevent integral windup by using the actuator limits in the inner loop and the velocity limits in the outer loop.

This paper is organized as follows. In Section 2, the system modeling is derived. In Section 3, the proposed controller is presented. The experimental setup and results are presented in Section 4. Finally, conclusion is drawn in Section 5.

II. System modelling

A. AUV modelling

The motion of the AUV can be described by using a body frame relative to a navigation frame (Fig. 1). The body frame is composed of the linear and angular velocities $[u\ v\ w\ p\ q\ r]$; the navigation frame is composed of the position and the orientation $[x\ y\ z\ \phi\ \theta\ \psi]$. In this paper, neglecting heave, roll and pitch motions, we consider the motions in the horizontal plane corresponding to motion components such as the linear and angular velocities $[u\ v\ r]$, and the position and orientation $[x\ \ y\ \ \psi]$. The 3-degree of freedom (DOF) horizontal plane model has been presented in [2], and the hydrodynamics of the AUV is described as follows:

$$m_u\dot{u} = m_v vr - k_u u - k_{u|u|}u|u| + F_u, \quad (1)$$

$$m_v\dot{v} = -m_u ur - k_v v - k_{v|v|}v|v| + F_v, \quad (2)$$

$$I_r\dot{r} = -(m_v - m_u)ur - k_r r - k_{r|r|}r|r| + T_r, \quad (3)$$

where u and v are the linear velocities in surge and sway, and r is the rotational velocity in yaw; m_u and m_v are the

This research was supported by the MKE(The Ministry of Knowledge Economy), Korea, under the "IT Consilience Creative Program" support program supervised by the NIPA(National IT Industry Promotion Agency) (C1515-1121-0003).

978-0-933957-40-4 ©2013 MTS

masses in surge and sway and I_r is the moment of inertia in yaw; $k_u/k_{u|u}$, $k_v/k_{v|v|}$ and $k_r/k_{r|r|}$ are the linear/quadratic damping coefficients in surge, sway and yaw, respectively; F_u and F_v are the external forces acting on the vehicle in surge and sway, respectively; and T_r is the external torque on the vehicle in yaw.

The kinematics of the AUV is described as follows:

$$\dot{x} = u\cos\psi - v\sin\psi, \tag{4}$$

$$\dot{y} = u\sin\psi + v\cos\psi, \tag{5}$$

$$\dot{\psi} = r, \tag{6}$$

where x, y and ψ are the position and the orientation in surge, sway and yaw motions, respectively.

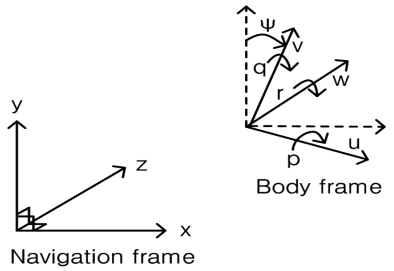

Fig. 1. The navigation and body frames.

B. Actuator modelling

Comparing to the AUV's time constant, the actuator system's time constant is small, so we neglect the actuator dynamics, and the resulting actuator system can be described as follows:

$$u_i = \begin{cases} c_{1i+}v_{ti}^2 + c_{2i+}v_{ti} + c_{3i+} & \text{if } v_{di+} < v_{ti} \\ 0 & \text{if } v_{di-} < v_{ti} \le v_{di+} \\ c_{1i-}v_{ti}^2 + c_{2i-}v_{ti} + c_{3i-} & \text{if } v_{ti} \le v_{di-} \end{cases}, \tag{7}$$

where u_i is its exerted force, v_{ti} is its input voltage, v_{di+} and v_{di-} are upper and lower bounds of each actuator deadzone, c_{1i+}, c_{2i+}, c_{3i+}, c_{1i-}, c_{2i-} and c_{3i-} are constants for $i = 1, ..., n$ with n being the number of the actuators.

III. Controller design

A. Dual-loop VSPID controller with anti-windup

Each motion in surge and sway is coupled with the motion in yaw, and each dynamics in surge and sway has nonlinearities. This coupling and nonlinearity can degrade the control performance and even cause the system to become unstable. To overcome this problem, we design the controller in surge and sway in conjunction with an autopilot for heading control and adopt the feedback linearization technique. Because we adopt these techniques, the coupling and nonlinearity terms do not affect the dynamics of the AUV, and the resulting dynamics in surge and sway are described as follows:

$$m_u\dot{u} = -k_u u + F_u, \tag{8}$$

$$m_v\dot{v} = -k_v v + F_v, \tag{9}$$

In this stage, we stabilize the above first-order dynamic systems by using the VSPID controller with anti-windup. The VSPID controller (Fig. 2) feeds the difference between the target input and force limits back to the integral term when the switching condition is satisfied, i.e.,

$$e_{i1} = \begin{cases} \frac{K_{p1}}{T_{i1}}e_1 + \alpha_1\bar{F} & \text{if } \bar{F} \neq 0 \text{ and} \\ & e_1(F^* - \frac{F_{max}+F_{min}}{2}) > 0 \\ \frac{K_{p1}}{T_{i1}}e_1 & \text{otherwise} \end{cases}, \tag{10}$$

where

$$\bar{F} = \begin{cases} F^* - F_{max} & \text{if } F_{max} < F^* \\ 0 & \text{if } F_{min} < F^* \le F_{max} \\ F^* - F_{min} & \text{if } F^* \le F_{min} \end{cases}, \tag{11}$$

α_1 is the design parameter, F_{max} is the maximum value of the force input, F_{min} is the minimum value of the force input, and $e_1 = V^* - V$ where V^* is the target velocity and V is the velocity. Comparing to the conventional anti-windup scheme with back-calculation, the anti-windup technique of the proposed controller can keep F close to $\bar{F}$ during saturation so that the controller returns to linear operation as fast as possible [12].

Finally, we stabilize the whole system including the kinematics by using the VSPID controller with anti-windup in the outer-loop (Fig. 3). The outer-loop controller structure is the same as the inner-loop controller structure. The main difference lies in using the velocity limits to implement the anti-windup. So, the outer-loop controller feeds the difference between the target velocity and the velocity limits back to the integral term when the switching condition is satisfied, i.e.,

$$e_{i2} = \begin{cases} \frac{K_{p2}}{T_{i2}}e_2 + \alpha_2\bar{V} & \text{if } \bar{V} \neq 0 \text{ and} \\ & e_2(V^* - \frac{V_{max}+V_{min}}{2}) > 0 \\ \frac{K_{p2}}{T_{i2}}e_2 & \text{otherwise} \end{cases}, \tag{12}$$

where

$$\bar{V} = \begin{cases} V^* - V_{max} & \text{if } V_{max} < V^* \\ 0 & \text{if } V_{min} < V^* \le V_{max} \\ V^* - V_{min} & \text{if } V^* \le V_{min} \end{cases}, \tag{13}$$

α_2 is the design parameter, V_{max} is the maximum value of the velocity, V_{min} is the minimum value of the velocity, and $e_2 = R - P$ where R is the reference command and P is the position signal. The schematic diagram of the AUV control system is shown in Fig. 4.

B. Force distribution

Because the number of actuators is larger than the controllable DOF in the AUV, we needs to distribute the control surface forces to each actuator. To do that, we define the constraint optimization problem as follows [13]:

$$\min_{\mathbf{u}} J = \frac{1}{2}\mathbf{u^T W u}$$
$$\text{subject to} \quad \mathbf{F = Bu}, \tag{14}$$

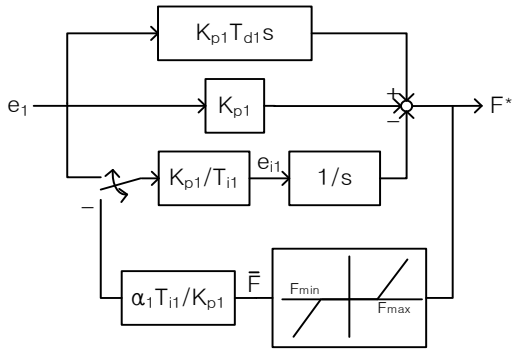

Fig. 2. Schematic diagram of VSPID controller with anti-windup in the inner-loop.

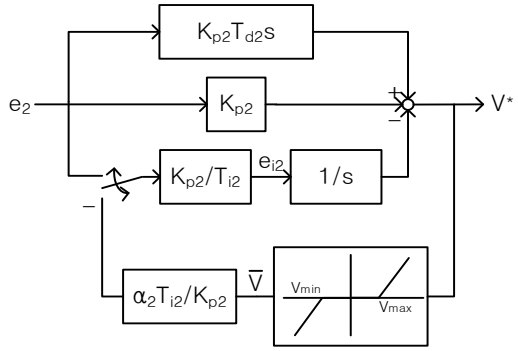

Fig. 3. Schematic diagram of VSPID controller with anti-windup in the outer-loop.

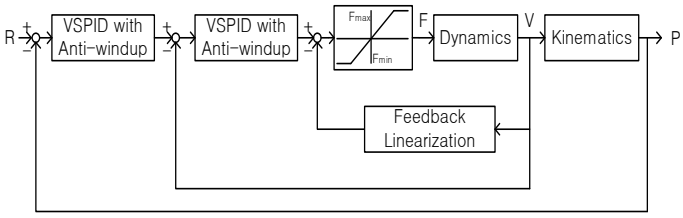

Fig. 4. Schematic diagram of AUV control system.

where $\mathbf{W}$ is the energy weighting matrix, $\mathbf{u} = [u_1 \ ... \ u_n]^T$ is the actuator force vector, $\mathbf{F} = [F_u \ F_v \ T_r]^T$ is the force/torque input vector, and $\mathbf{B}$ is the actuator force/torque distribution matrix. If $\mathbf{BW^{-1}B^T}$ is nonsingular, one can easily show that

$$\mathbf{F} = \mathbf{B}^{\dagger}\mathbf{u}, \tag{15}$$

where $\mathbf{B}^{\dagger} = \mathbf{W^{-1}B^T}(\mathbf{BW^{-1}B^T})^{-1}$. When all actuators are equally weighted, i.e., $\mathbf{W} = \mathbf{I}$, the generalized inverse becomes $\mathbf{B}^{\dagger} = \mathbf{B^T}(\mathbf{BB^T})^{-1}$.

Remark 1. To tune the inner-loop PID controller gains, we use the characteristic polynomial for the closed-loop system as follows [14]:

$$s^2 + (a + bK_{p1})s + bK_{p1}/T_{i1}, \tag{16}$$

where $a = k_u/m_u$ or k_v/m_v, and $b = 1/m_u$ or $1/m_v$. Assuming that the desired characteristic polynomial is

$$s^2 + 2\zeta w_0 s + w_0^2, \tag{17}$$

the controller parameters need to become

$$K_{p1} = \frac{2\zeta w_0 - a}{b}, \tag{18}$$

$$T_{i1} = \frac{b}{w_0^2} K_{p1}. \tag{19}$$

The parameters w_0 and ζ determine the response speed and the damping, respectively.

IV. Experiment

A. Experimental setup

To demonstrate the feasibility of developed controller, it is applied to Cyclops (Fig. 5), an AUV developed at the Hazardous Environmental Robotics Laboratory at the Pohang University of Science and Technology (POSTECH). This AUV is equipped with two actuators for surge motion, two actuators for heave motion, four actuators for sway and yaw motion, a Doppler velocity log for measuring the positions and the velocities, and a fiber-optic gyro unit for measuring the heading and the yaw rate. The developed controller is implemented in a computer system in Cyclops at a 100-ms sampling interval. The computer system consists of two PC104 modules. The real time operating system that runs on the computer system is Windows XP. The controller is programmed using Visual Studio 2008.

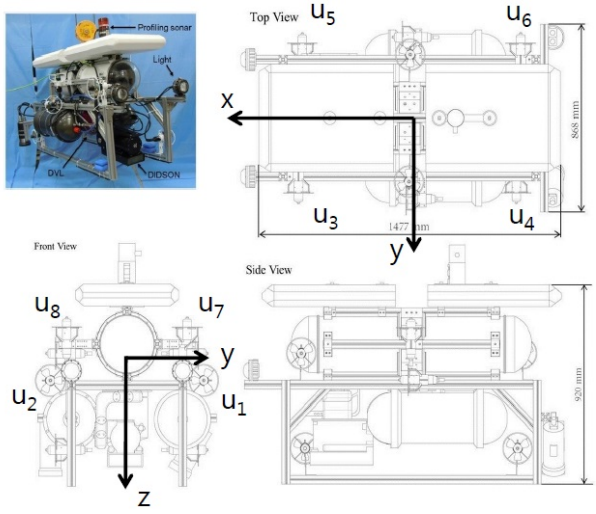

Fig. 5. Structure of Cyclops underwater vehicle.

Surge and sway motion control tests were carried out in an engineering basin in conjunction with the autopilot for heading control (Fig. 6). The engineering basin is located at the Korea Institute of Robotics and Convergence, and its size is about 12x8x6 m [15].

In the proposed control scheme, the each VSPID controller is used in both the inner- and outer-loops for both surge and sway directions. The gains of inner-loop VSPID controllers were obtained based on the parameters: $\zeta = 2.5$, $w_0 = 0.01$,

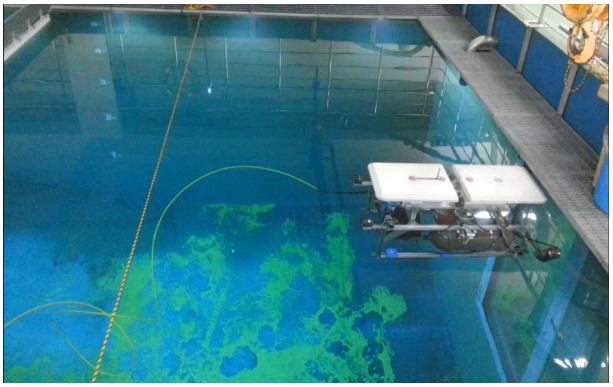

Fig. 6. Cyclops underwater vehicle in the engineering basin.

$\alpha_1 = 0.01$ in surge and $\zeta = 21$, $w_0 = 0.005$, $\alpha_1 = 0.01$ in sway. The gains of outer-loop VSPID controllers were obtained experimentally as $K_{p2} = 0.5$ $T_{d2} = 0$, $T_{i2} = 2500$, $\alpha_2 = 0.0015$ in surge and $K_{p2} = 0.7$, $T_{d2} = 0$, $T_{i2} = 700$, $\alpha_2 = 0.002$ in sway.

By using each actuator's limits, the force limits can be easily obtained as $F_{max} = 2$ and $F_{min} = -2$ in surge, and $F_{max} = 4$ and $F_{min} = -4$ in sway. By applying the maximum force input to the AUV in surge and sway directions, we can obtain the velocity limits as $V_{max} = 2$ and $V_{min} = -2$ in surge, and $V_{max} = 3$ and $V_{min} = -3$ in sway.

The actuator force/torque distribution matrix $\mathbf{B}$ is defined as

$$\mathbf{B} = \begin{bmatrix} 1 & 1 & 0 & 0 & 0 & 0 \\ 0 & 0 & 1 & 1 & -1 & -1 \\ 0 & 0 & d_c \sin(\theta_c) & -r_c \sin(\theta_c) & -r_c \sin(\theta_c) & r_c \sin(\theta_c) \end{bmatrix}. \quad (20)$$

where r_c is the distance from the center of gravity of the AUV to the point where each actuator force acts, and θ_c is the angle between position and force vectors. Here, $r_c = 580\ mm$ and $\theta_c = 115.5°$. The actuator force vector $\mathbf{u} = [u_1\ ...\ u_6]^T$ where u_1 and u_2 are the actuator forces for surge motion, u_3, u_4, u_5 and u_6 are the actuator forces for sway motion (Fig. 5). The energy weighting matrix $\mathbf{W}$ is the identity matrix.

Other controller parameters were determined based on the actual measurements and system identification techniques and are listed (Tables I and II).

B. Experimental results

We applied the developed controller to the real AUV. Under the above parameter settings and step input command ($R = 1$ m), the command input response in surge direction shows the large percentage overshoot and long settling time with the dual-loop VSPID controller without anti-windup (Fig. 7). On the other hand, the command input responses have a small percentage overshoot and short settling time with the dual-loop VSPID controller with anti-windup. The command input responses in sway show similar results, but the response with anti-windup techniques shows not only a small overshoot but also an undershoot due to the large value α_1 in sway (Fig. 8).

TABLE I
CONTROLLER PARAMETER VALUES.

The controller parameter	Value
Weight of Cyclops in air m (kg)	219.8
Length of Cyclops l (mm)	1477
Width of Cyclops w (mm)	868
Height of Cyclops h (mm)	920
Mass of Cyclops in surge m_u (kg)	391.5
Linear drag coefficient in surge k_u	16
Quadratic drag coefficient in surge $k_{u\|u\|}$	229.4
Mass of Cyclops in sway m_v (kg)	639.6
Linear drag coefficient in sway k_v	131.8
Quadratic drag coefficient in sway $k_{v\|v\|}$	328.3

TABLE II
ACTUATOR PARAMETER IDENTIFICATION RESULTS.

Actuator number	c_{1+}	c_{2+}	c_{3+}	v_{d+}
1	0.3027	-0.4609	0.1516	0.5
2	-0.2978	0.4097	-0.1413	0.5
3	-0.3256	0.5468	-0.2179	0.5
4	-0.3524	0.6428	-0.3325	0.5
5	0.3168	-0.4875	0.1412	0.5
6	0.3304	-0.5153	0.1859	0.5
Actuator number	c_{1-}	c_{2-}	c_{3-}	v_{d-}
1	-0.3266	-0.5388	-0.2919	-0.5
2	0.2867	0.3047	0.033	-0.5
3	0.2889	0.3873	0.086	-0.5
4	0.2744	0.3703	0.099	-0.5
5	-0.2986	-0.3567	-0.075	-0.5
6	-0.2673	-0.3137	-0.073	-0.5

To compare the performance of various controllers numerically, we define the percentage overshoot as the maximum value minus the step value divided by the step value, and the settling time as the required time for the response curve to reach and stay within a range of 5% of the final value.

We examined the percentage overshoot and the setting time of various controllers (Tables III and IV). The dual-loop VSPID controller with anti-windup achieves the smallest percentage overshoot and the shortest settling time among the three controllers and can be qualified as a good controller candidate.

TABLE III
THE OVERSHOOT AND THE SETTING TIME OF THE COMMAND INPUT RESPONSES IN SURGE.

Controller	Percentage Overshoot (%)	Settling time (s)
VSPID	42.2	28.3
VSPID+Anti-windup in the inner-loop only	10.2	21.1
VSPID+Anti-windup	6.0	14.4

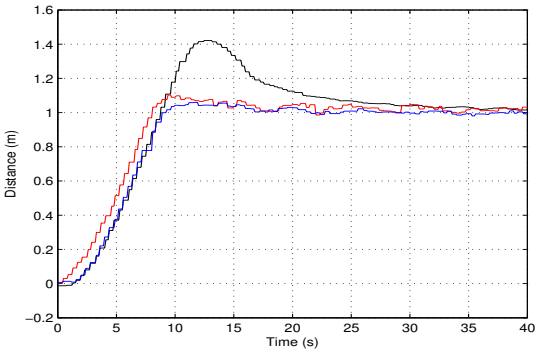

Fig. 7. The command input responses in surge. Black line: the command input response with VSPID controller; Red line: the command input response with VSPID controller with anti-windup in the inner-loop only; Blue line: the command input response with VSPID controller with anti-windup.

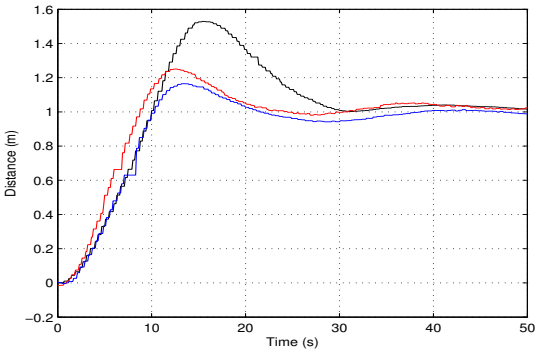

Fig. 8. The command input responses in sway. Black line: the command input response with VSPID controller; Red line: the command input response with VSPID controller with anti-windup in the inner-loop only; Blue line: the command input response with VSPID controller with anti-windup.

TABLE IV
THE OVERSHOOT AND THE SETTING TIME OF THE COMMAND INPUT RESPONSES IN SWAY.

Controller	Percentage Overshoot (%)	Settling time (s)
VSPID	52.9	27.9
VSPID+Anti-windup in the inner-loop only	25.0	39.4
VSPID+Anti-windup	16.5	31.2

V. CONCLUSION

In this paper, we introduce the dual-loop VSPID controller with anti-windup to reduce the integral-windup effect. To the best of our knowledge, this is the first attempt to use the anti-windup technique in the dual-loop PID controller. The performance of the proposed controller was tested using the real AUV in surge and sway. The experimental result shows that the proposed controller significantly reduced the overshoot as well as the settling time.

REFERENCES

[1] B. Jarving, "The NDRE-AUV flight control system," Oceanic Engineering, vol. 19, no. 4, pp. 497 - 501, 1994.

[2] M. Caccia and G. Veruggio, "Guidance and control of a reconfigurable unmanned underwater vehicle," Control Engineering Practice, vol. 8, no. 1, pp. 21 - 37, 2000.

[3] A. Healey and D. Lienard, "Multivariable sliding mode control for autonomous diving and steering of unmanned underwater vehicles," Oceanic Engineering, vol. 18, no. 3, pp. 327 - 339, 1993.

[4] L. Rodrigues, P. Tavares, M. Prado, "Sliding mode control of an AUV in the diving and steering planes," Proceedings of OCEANS'96, pp 576 - 583, 1996.

[5] C. Silverstre and A. Pascoal, "Control of the INFANTE AUV using gain scheduled static output feedback," Control Engineering Practice, vol. 12, no. 12, pp. 1501 - 1509, 2004.

[6] Z. Feng and R. Allen, "Reduced order H_∞ control of an autonomous underwater vehicle," Control Engineering Practice, vol. 12, no. 12, pp. 1511 - 1520, 2004.

[7] J. H. Li and P. M. Lee, "Design of an adaptive nonlinear controller for depth control of an autonomous underwater vehicle," Oceanic Engineering, vol. 32, pp. 2165 - 2181, 2005.

[8] S. Miyamoto, T. Aoki, T. Maeda, K. Hirokawa, T. Ichikawa, T. Saitou, H. Kobayashi, E. Kobayashi, and S. Iwasaki, "Maneuvering control system design for autonomous underwater vehicle," MTS/IEEE Conference and Exhibition, vol. 1, pp. 482 - 489, 2001.

[9] J. Folcher, "Steering control of an underwater vehicle: An anti windup design," Proceedings of the 13th International Symposium on Unmanned Untethered Submersible Technology, pp. 173 - 179, 2003.

[10] R. M. C. De Keyser, "Improved mould-level control in a continuous steel casting line," Control Engineering Practice, vol. 5 no. 2, 231 - 237, 1997.

[11] A. S. Hodel and C. E. Hall, "Variable-structure PID Control to prevent integrator windup," IEEE Transactions on Industrial Electronics, vol. 48, no. 2, pp. 442 - 451, 2001.

[12] A. Visioli. Practical PID control. Springerverlag London Limited, 2006.

[13] T. I. Fossen, "Guidance and control of ocean control," London, U.K.:Wiley, 1994

[14] B. C. Kuo and M. F. Golnaraghi, "Automatic control systems," New York: John Wiley & Sons, 2003.

[15] J. H. Li, B. H. Yoon, S. S. Oh, J. S. Cho, J. G. Kim, M. J. Lee, and J. W. Lee, "Development of an intelligent autonomous underwater vehicle," P-SURO. In OCEANS 2010 IEEE-Sydney, pp. 1 - 5, 2010.